Central European Journal of Energetic Materials
ISSN 1733-7178; e-ISSN 2353-1843

Cent. Eur. J. Energ. Mater. 2017, *14*(2): 430-447 DOI: 10.22211/cejem/70728

The Catalytic Effect of Mn_2O_3 Nanoparticles on the Ignition Reaction of Pyrotechnic of Ammonium Nitrate(V)/Thiourea

Hamid Reza Pouretedal,* Mohsen Ravanbod**

Faculty of Applied Chemistry, Malek-ashtar University of Technology, Shahin-Shahr, Iran
*E-mail: *HR_POURETEDAL@mut-es.ac.ir, **mravanbod@mut-es.ac.ir*

Abstract: The non-isothermal TG/DSC technique has been used to study the kinetic triplet and heat of ignition reaction of ammonium nitrate(V) (AN)/thiourea (TU) pyrotechnic in the presence of Mn_2O_3 catalyst nanoparticles under an argon atmosphere at different heating rates (5 $K \cdot min^{-1}$, 10 $K \cdot min^{-1}$, 15 $K \cdot min^{-1}$ and 20 $K \cdot min^{-1}$). The activation energies for the ignition reaction of AN/TU were calculated using the non-isothermal isoconversional Kissinger-Akahira-Sunose (KAS) and Friedman equations for different conversion fraction (α) values in the range 0.1-0.9. The pre-exponential factor and kinetic model were determined by means of the compensation effect and the selected model was confirmed by a nonlinear fitting method. The average activation energies in the absence and presence of 5 wt.% Mn_2O_3 nanoparticles were 110.1 $kJ \cdot mol^{-1}$ to 117.3 $kJ \cdot mol^{-1}$ for the reaction model A_3 ($g(\alpha)=[-\ln(1-\alpha)]^{1/3}$), and 86.5 $kJ \cdot mol^{-1}$ to 101.8 $kJ \cdot mol^{-1}$ for the reaction model A_4 ($g(\alpha)=[-\ln(1-\alpha)]^{1/4}$). The evolved heat ($\Delta H$) of ignition reaction in the presence of Mn_2O_3 was about 4 times that in the absence of the nano-sized Mn_2O_3.

Keywords: ammonium nitrate(V), thiourea, non-isothermal kinetic, ignition reaction, Mn_2O_3 nanoparticles

1 Introduction

A pyrotechnic composition is typically a finely divided mixture of organic or inorganic oxidizers and fuels designed to produce heat, light, sound, smoke or their combination [1]. The oxidizers are usually oxygen rich ionic solids which are used in pyrotechnic and propellant compositions to facilitate the process

of ignition by producing oxygen [2]. Ammonium nitrate(V) (AN, NH_4NO_3) is a well-known oxidizer used in pyrotechnic and propellant formulations [3-5]. Pure AN is not an explosive compound but the addition of a small amount of a suitable organic or inorganic compound makes the mixture capable of explosion [6]. Due to its suitable properties [7] such as chemical stability, low cost, low melting point (169.6 °C), low sensitivity to friction and shock, and also the fact that it undergoes almost 100% conversion to gaseous products upon reaction, AN has been extensively used in various energetic materials compositions. Also, thiourea (TU) has been used as a fuel in pyrotechnic compositions, such as in combination with potassium chlorate(V) [8].

The thermal decomposition and kinetic behavior of pyrotechnic compositions can be significantly improved by the presence of metals and metal oxides, especially if they are in nano-sized forms [9-11]. Among the metal oxide catalysts, nanoparticles of transition metal oxides such as ferric(III) oxide (Fe_2O_3) and manganese oxides (MnO_2 or Mn_2O_3) are highly effective in improving the decomposition of oxidizers [12-14].

In this study, a new pyrotechnic composition (AN/TU) is presented and the effect of synthesized Mn_2O_3 nanoparticles on the thermal decomposition of the mixture is evaluated systematically using TG/DSC analysis under an argon atmosphere at different heating rates (5 $K \cdot min^{-1}$, 10 $K \cdot min^{-1}$, 15 $K \cdot min^{-1}$, and 20 $K \cdot min^{-1}$). To the best of the authors' knowledge, no study has yet been reported on the reaction of AN/TU compositions. In the present work, the ICTAC Kinetic Committee recommendations [15] were used for a reliable estimation of the kinetic parameters. The activation energies were computed using the isoconversional Kissinger-Akahira-Sunose (KAS) and Friedman equations [16-18]. The pre-exponential factors and kinetic model functions were determined by means of the compensation effect and the selected model was confirmed using a nonlinear fitting method. Also, the enthalpy of the ignition reaction was calculated using the ASTM E537 method [19].

2 Experimental

2.1 Materials

All the chemicals used in this study were of analytical grade (purity > 99%) purchased from Merck Company and used as-received without further purification. De-ionized water (0.054 $\mu S \cdot cm^{-1}$) was used for preparation of aqueous solutions.

2.2 Synthesis of the materials

2.2.1 Synthesis of Mn_2O_3 nanoparticles by co-precipitation method

The preparation of Mn_2O_3 (Mn(III) oxide) nanoparticles was based on our previously reported method [20]. Manganese(II) sulfate and oxalic acid solutions (both 0.05 mol·L^{-1}) were mixed thoroughly by stirring at a constant temperature of 60 °C, followed by drop-wise addition of ammonia solution under continuous stirring until the solution pH reached 9.3. Stirring was continued for 1 h at the same temperature. The resulting brown precipitate was filtered and washed thoroughly with water. The precipitate was dried overnight at 95 °C. The dry powder was ground in a zirconium carbide mortar for 15 min to produce a fine powder. Finally, the fine powder was calcined in a furnace at 500 °C for 4 h.

2.2.2 Preparation of micro-sized ammonium nitrate and thiourea

Ammonium nitrate(V) and thiourea were milled separately in air using a Fritsch ball mill, model Mini Mill II, using a vessel and balls made of zirconium carbide (ZrC). The ball-milling was carried out using the following conditions: rotation speed, 300 rpm; powder-to-ball weight ratio, 1:20; milling time, 10 min. The fine powders produced were dried at 80 °C for 2 h and then sieved using a 45 μm sieve before preparing the test samples.

2.3 Preparation of the samples for thermal analysis

A mixture of fuel-rich AN/TU (50/50 wt.%) was prepared by intimately mixing the powders in a mortar for about 30 min. The synthesized nano Mn_2O_3 was added to the AN/TU (50/50 wt.%) mixture in a 5:95 mass ratio and the mixture was thoroughly mixed in the mortar for about 30 min.

2.4 Characterization of the nanoparticles

The X-ray diffraction (XRD) pattern of the nanoparticles was obtained using a Bruker D8 Advance powder diffractometer using Ni filtered Cu K_α radiation ($\lambda = 1.54056$ Å). The surface morphology of the products was characterized using a COXEM scanning electron microscope (SEM) with an accelerating voltage of 25 kV. Prior to the test, the powder samples were gold coated for 30 s in an ion sputtering unit (COXEM) to reduce the effect of charging. The Brunauer-Emmett-Teller (BET) surface area of the synthesized nanoparticles was determined by N_2 adsorption using a COSTECH sorptometer instrument, model KELVIN 1042 (Italy).

2.5 Thermal analysis conditions

The TG measurements were carried out using a Perkin Elmer simultaneous thermal analyzer, model STA 6000 (USA). Alumina sample vessels were used (70 μL volume) with alumina powder as the reference material. An argon atmosphere was created during the analysis (flow rate of 20 $mL \cdot min^{-1}$). For kinetic studies of the thermal decomposition, thermal analysis experiments were performed at heating rates of 5 $K \cdot min^{-1}$, 10 $K \cdot min^{-1}$, 15 $K \cdot min^{-1}$, and 20 $K \cdot min^{-1}$. In each experiment, approximately 3.5 mg sample was taken and heated from ambient temperature (25 °C) to 900 °C.

3 Results and Discussion

3.1 Characterization of the synthesized Mn_2O_3 nanoparticles

The XRD pattern of the nano-sized Mn_2O_3 synthesized by a co-precipitation method is shown in Figure 1. From the XRD diffractograms, it is clear that the synthesized metal oxide nanoparticles are purely crystalline in nature. The diffraction peaks at 2θ of 23.0°, 32.9°, 38.3°, 45.1°, 49.5°, 55.3°, and 65.7° confirm the cubic structure of the Mn_2O_3 particles [21].

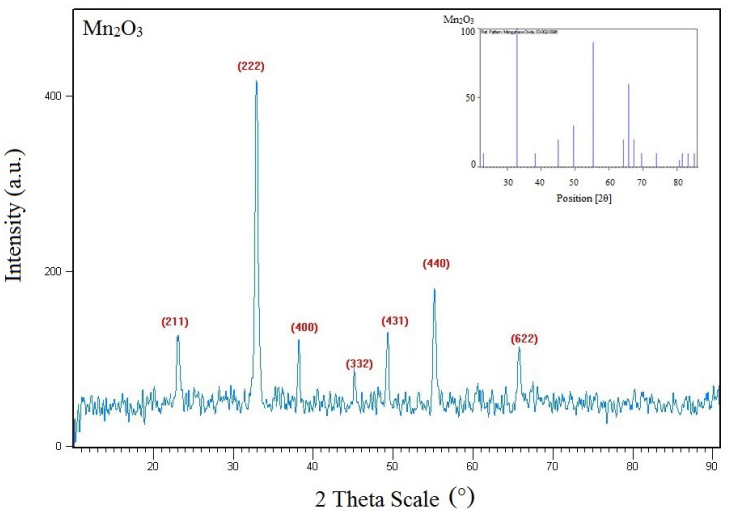

Figure 1. The XRD patterns of nano-sized Mn_2O_3 and its stick pattern

The crystallite size of the nanoparticles was calculated using Scherrer's equation [22]. The average crystallite size for Mn_2O_3 nanoparticles estimated

by this method and based on the highest peaks in the XRD spectrum (plane 222) was 27.7 nm.

The surface morphology of the synthesized nano metal oxide was obtained using a SEM (Figure 2). The image shows that the metal oxide consists of agglomerated particles with an average particle size of less than 100 nm.

The BET measurement showed that the specific surface area of the Mn_2O_3 nanoparticles was 35.6 $m^2 \cdot g^{-1}$.

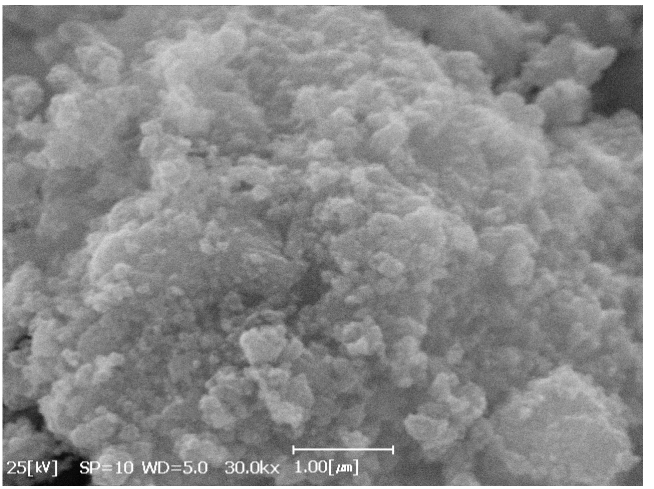

Figure 2. SEM image of the Mn_2O_3 nanoparticles

3.2 Thermal analysis

3.2.1 Thermal behavior of pure AN and TU

The TG/DSC curves for the thermal decomposition of pure ammonium nitrate(V) and thiourea at a heating rate of 10 $K \cdot min^{-1}$ under an argon atmosphere are presented in Figures 3 and 4, respectively. From the DSC thermogram shown in Figure 3, the two first endothermic peaks observed around 56 °C and 126 °C are due to phase transitions in AN and the sharp endothermic peak at approximately 168 °C can be assigned to the melting point of AN [23]. A broad endothermic peak related to decomposition is observed at a peak temperature of 265 °C. The TG curve also shows that after AN melts, decomposition occurs with a mass reduction of about 100% according to the following reaction (Eq. 1) [23]:

$$NH_4NO_3\,(l) \rightarrow NH_3\,(g) + HNO_3\,(g) \qquad (1)$$

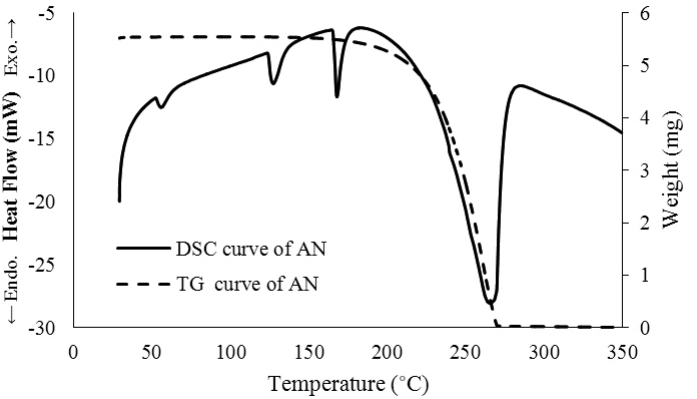

Figure 3. TG/DSC curves for ammonium nitrate at heating rate of 10 $K \cdot min^{-1}$

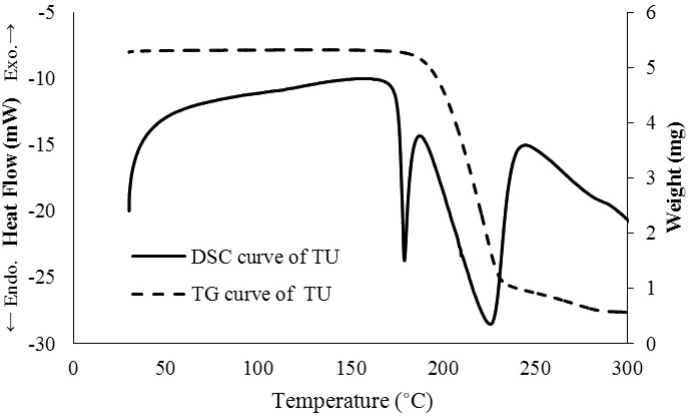

Figure 4. TG/DSC curves for thiourea at heating rate of 10 $K \cdot min^{-1}$

The DSC thermogram of pure TU in Figure 4 shows two overlapping endothermic peaks in which the first sharp endothermic peak (with its maximum at 179 °C) is related to the melting point of TU. The broad endothermic process (peak temperature 225 °C) is due to decomposition of TU [24]. The TG thermogram for TU shows that similarly to AN, TU starts to decompose after it melts. Among the possible gaseous products from the thermal decomposition of TU, two product pairs including ammonia + isothiocyanic acid, and hydrogen sulfide + carbodiimide can be generated according to the following reactions (Eq. 2 and Eq. 3) [25]:

$$SC(NH_2)_2\,(s) \rightarrow NH_3\,(g) + HN{=}C{=}S\,(g) \quad (2)$$

$$SC(NH_2)_2\,(s) \rightarrow H_2S\,(g) + HN{=}C{=}NH\,(g) \quad (3)$$

3.2.2 Thermal behavior of the mixtures

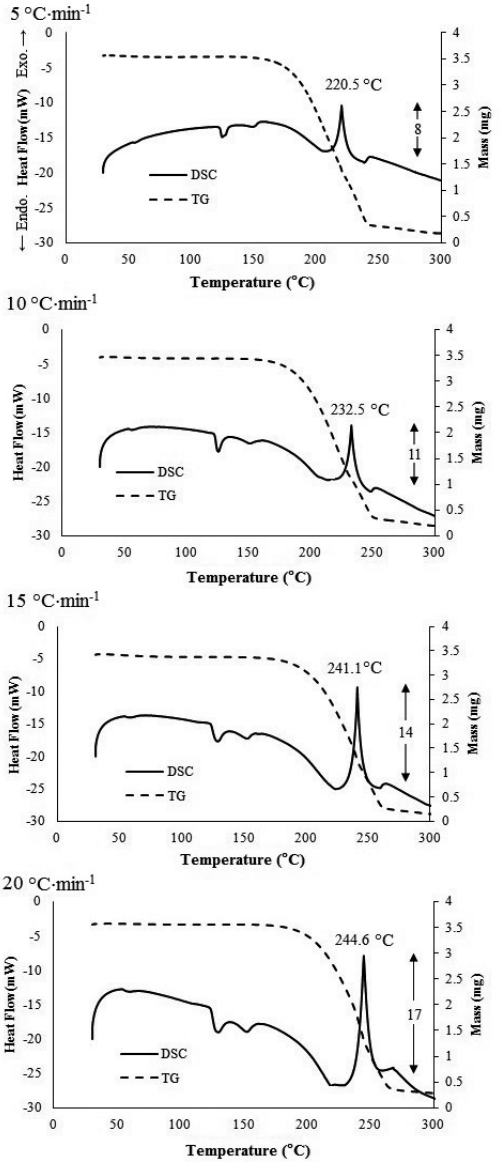

Figure 5. TG/DSC curves for AN/TU (50/50 wt.%) at different heating rates in an argon atmosphere

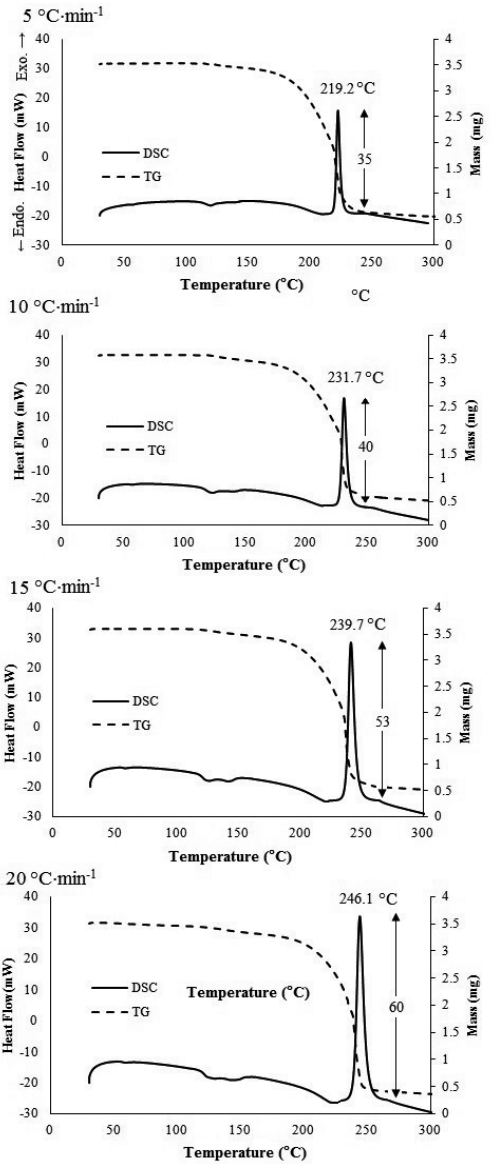

Figure 6. TG/DSC curves for AN/TU/Mn_2O_3 (47.5/47.5/5 wt.%) at different heating rates in an argon atmosphere

The TG/DSC curves for the AN/TU mixture (50/50 wt.%) heated at different heating rates (5 K·min^{-1}, 10 K·min^{-1}, 15 K·min^{-1}, and 20 K·min^{-1}) under an argon atmosphere are shown in Figure 5. The DSC curves indicate two consecutive

endothermic peaks at about 126 °C and 153 °C, which can be assigned to the phase transition temperature and melting point of ammonium nitrate(V) in the AN/TU mixture. The observed exothermic peak is assigned to the ignition reaction of AN/TU according to the following reaction (Eq. 4):

$$2NH_4NO_3\,(l) + SC(NH_2)_2\,(l) \rightarrow CO_2\,(g) + SO_2\,(g) + 2NO\,(g) + 4NH_3\,(g) \qquad (4)$$

Despite the fact that the thermal decomposition of AN and TU are endothermic, an exothermic pattern was observed during the reaction between AN and TU in the DSC curves. As the heating rates increase, the exothermic peaks for the ignition process shift to higher temperatures (220.5 °C, 232.5 °C, 241.1 °C and 244.6 °C, for heating rates of 5 $K \cdot min^{-1}$, 10 $K \cdot min^{-1}$, 15 $K \cdot min^{-1}$, and 20 $K \cdot min^{-1}$, respectively) and the corresponding reaction peak heights enhance.

The TG/DSC curves for the AN/TU/Mn_2O_3 mixture containing 5 wt.% Mn_2O_3 nanoparticles (47.5/47.5/5 wt.%) at different heating rates (5 $K \cdot min^{-1}$, 10 $K \cdot min^{-1}$, 15 $K \cdot min^{-1}$, and 20 $K \cdot min^{-1}$) under an argon atmosphere are shown in Figure 6. Similar to the DSC thermogram of the AN/TU mixture, two weak endothermic peaks were observed around 120 °C and 150 °C followed by a sharp exothermic peak. We assigned the observed exothermic peak to the ignition reaction of AN/TU in the presence of nano sized Mn_2O_3. As the heating rate was increased (5 $K \cdot min^{-1}$, 10 $K \cdot min^{-1}$, 15 $K \cdot min^{-1}$, and 20 $K \cdot min^{-1}$), the exothermic peak for the ignition process shifted to higher temperatures (219.2 °C, 231.7 °C, 239.7 °C, and 246.1 °C, for heating rates of 5 $K \cdot min^{-1}$, 10 $K \cdot min^{-1}$, 15 $K \cdot min^{-1}$, and 20 $K \cdot min^{-1}$, respectively) and the intensity of the corresponding reaction peak increased.

Comparison of the DSC curves in Figures 5 and 6 shows that the peak height for the ignition reaction in the presence of Mn_2O_3 nanoparticles is about 4 times that for the composition without the metal oxide. This behavior reveals that the presence of Mn_2O_3 nanoparticles in the mixture causes the reaction between AN and TU to be more complete and/or the reaction products are changed. The following equation (Eq. 5) is suggested for the reaction between AN and TU in the presence of Mn_2O_3 nanoparticles:

$$3NH_4NO_3\,(l) + SC(NH_2)_2\,(l) \xrightarrow{Mn_2O_3} CO_2\,(g) + SO_2\,(g) + 5H_2O\,(g) + \\ + 2NH_3\,(g) + 3N_2\,(g) \qquad (5)$$

The enthalpies ($\Delta H/J \cdot g^{-1}$) for the ignition reaction of AN/TU in the presence and absence of nano Mn_2O_3 at different heating rates, calculated using the ASTM E537 method, are given in Table 1. As can be seen, the average heats evolved

from the ignition reaction of AN/TU are 360 J·g^{-1} and 95 J·g^{-1} in the presence and absence of nano metal oxide, respectively. The results indicate that the type of reaction products was changed by the presence of Mn_2O_3 in the mixture.

Table 1. The enthalpies (ΔH, J·g^{-1}) and their uncertainties for ignition reaction of AN/TU in the presence and absence of nano metal oxide at different heating rates calculated using ASTM E537

Heating rate, β [K·min^{-1}]	Enthalpy, ΔH [J·g^{-1}] in the presence of Mn_2O_3	Enthalpy, ΔH [J·g^{-1}] in the absence of Mn_2O_3
5	387	81
10	368	82
15	348	106
20	338	112
Average	360 ± 22	95 ± 16

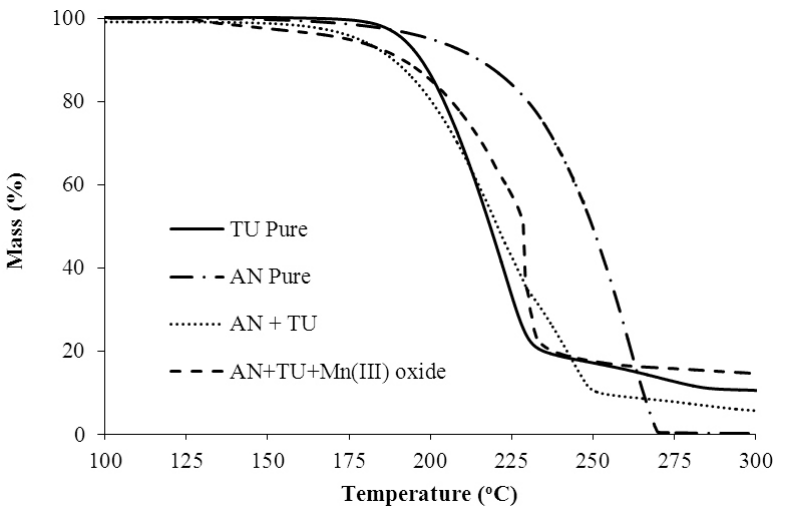

Figure 7. TG curves of different samples at heating rate of 10 °C·min^{-1}

The theoretical calculations of the heat of reaction based on bond energy [26] indicate that ΔH of reactions (4) and (5) are approximately –95 kcal·mol^{-1} and −414 kcal·mol^{-1}, respectively. These results (*i.e.* increasing of reaction heat by about 4 times in the presence of Mn_2O_3) are in agreement with the experimental results (*i.e.* 360 J·g^{-1} and 95 J·g^{-1} in the presence and absence of nano Mn_2O_3) and verify the suggested reaction equations. However, the theoretical and experimental values of the heat of reaction are different from each other and this

can be related to the conditions of reaction.

The TG curves in Figures 5 and 6 show that before the start of AN/TU reaction, there is a mass loss process which can be related to the thermal decomposition of TU. This process can be also described by the TG curves presented in Figure 7. Thus, the ignition reaction of AN/TU mixtures started with the decomposition of ammonium nitrate.

3.3 Kinetics of the solid-state reactions

The rate of processes in the solid-state is generally described by the following equation (Eq. 6):

$$\frac{d\alpha}{dt} = A \cdot \exp[\frac{-E_\alpha}{RT}] \cdot f(\alpha) \tag{6}$$

where α is the conversion fraction, t is time, A (min^{-1}) is the pre-exponential (frequency) factor, E_α is the activation energy as a function of α ($kJ \cdot mol^{-1}$), R is the universal gas constant (8.314 $J \cdot mol^{-1} \cdot K^{-1}$), T is absolute temperature (K), and $f(\alpha)$ is the reaction model function depending on the particular decomposition mechanism [27, 28].

The activation energy (E_α), the pre-exponential factor (A), and the reaction model function $f(\alpha)$ are called the kinetic triplet. The kinetic triplet is required for prediction of the thermal stability of the materials under various applied temperatures and is needed to provide a mathematical description of the process [29].

3.3.1 Calculation of the activation energy by Model-free Isoconversional Method

According to the ICTAC Kinetic Committee recommendations [15], the activation energies (E_α) were calculated by the KAS and Friedman methods based on DSC data at multiple heating rates (5 $K \cdot min^{-1}$, 10 $K \cdot min^{-1}$, 15 $K \cdot min^{-1}$, and 20 $K \cdot min^{-1}$). The KAS and Friedman methods can be expressed in Eq. 7 and Eq. 8, respectively:

$$\ln(\frac{\beta_i}{T_{\alpha,i}^2}) = \text{Const} - (\frac{E_\alpha}{RT_\alpha}) \tag{7}$$

$$\ln[\beta_i(\frac{\mathrm{d}\alpha}{\mathrm{d}T})_{\alpha,i}] = \ln[f(\alpha)A_\alpha] - (\frac{E_\alpha}{RT_{\alpha,i}}) \tag{8}$$

The activation energy values can be obtained from the slope of plots of

$\ln(\beta_i/T^2_{\alpha,i})$ versus $1/T_\alpha$ (Eq. 7) and $\ln[\beta_i\,(d\alpha/dT)_{\alpha,i}]$ versus $1/T_{\alpha,i}$ (Eq. 8) by linear regression using the least-squares method.

Table 2. The activation energies (E_α, kJ·mol^{-1}) and their standard deviations calculated using KAS and Friedman methods for the ignition reaction of AN/TU in the presence and absence of nano sized Mn_2O_3 at different α values

α	AN/TU/Mn_2O_3				AN/TU			
	KAS		Friedman		KAS		Friedman	
	E_α [kJ·mol^{-1}]	R^2	E_α [kJ·mol^{-1}]	R^2	E_α [kJ·mol^{-1}]	R^2	E_α [kJ·mol^{-1}]	R^2
0.1	104.64	0.999	85.84	0.990	108.25	0.992	115.12	0.998
0.2	103.54	0.999	84.84	0.992	108.92	0.993	116.15	0.999
0.3	102.84	0.999	85.07	0.994	109.36	0.994	116.75	0.999
0.4	102.25	0.999	85.16	0.995	109.73	0.994	117.17	0.999
0.5	101.72	0.999	85.76	0.995	110.05	0.994	117.53	0.999
0.6	101.20	0.999	86.32	0.995	110.38	0.995	117.82	0.999
0.7	100.63	0.999	87.04	0.994	110.74	0.995	118.13	0.999
0.8	99.94	0.999	88.22	0.993	111.19	0.995	118.36	0.999
0.9	99.00	0.999	90.54	0.992	111.86	0.996	119.01	1.000
Average	101.8±1.8	0.999	86.5±1.8	0.993	110.1±1.1	0.994	117.3±1.2	0.999

The activation energies for ignition reactions of AN/TU mixtures in the presence and absence of Mn_2O_3 nanoparticles were calculated based on DSC peak area at different heating rates of 5 K·min^{-1}, 10 K·min^{-1}, 15 K·min^{-1}, and 20 K·min^{-1} for different α values in the range of 0.1-0.9. The activation energies obtained by the KAS and Friedman methods are listed in Table 2. As seen, the average values of E_α for ignition reaction of AN/TU/Mn_2O_3 mixtures in the present work calculated by the KAS and Friedman methods were 101.8 ± 1.8 kJ·mol^{-1} and 86.5 ± 1.8 kJ·mol^{-1}, respectively, which are close to each other and smaller than the activation energy values related to the (50/50) AN/TU mixture, *i.e.* 110.1 ± 1.1 kJ·mol^{-1} and 117.3 ± 1.2 kJ·mol^{-1} obtained by the KAS and Friedman methods, respectively. The results reveal that Mn_2O_3 nanoparticles exert catalytic activity on the ignition reaction of the AN/TU mixture.

The mechanism of the catalytic action of Mn_2O_3 can be discussed based on the activity of the metal cation in forming a surface complex with nitrate anions.

The catalytic activity of the metal oxides is related to their electron configuration [30, 31]. The metal cations in Mn_2O_3 with partially filled d-orbitals have unfilled valence orbitals and relatively small size because of low electrical shielding. Therefore, they have a high tendency to attract extra electrons or negative charges and behave as Lewis acid sites [32]. On the other hand, the oxygen atoms in the nitrate anion (NO_3^-) have unshared electron pairs, and thus behave as Lewis bases donating their unshared electron pairs to the empty valence orbitals of the metal cations of the oxide catalyst to form a surface complex. Formation of the M−O coordination bond weakens the O−N bond in the NO_3^- group and thereby facilitates the decomposition process of AN [20].

3.3.2 Determination of the kinetic triplet by Model-fitting Method

In order to select the reaction model, different kinetic functions [29] of the common models in solid-state reactions were tested with the Kennedy and Clark model fitting method as following (Eq. 9) [33]:

$$\ln\left[\frac{\beta \cdot g(\alpha)}{(T-T_0)}\right] = \ln A - \frac{E_a}{RT} \tag{9}$$

According to Eq. 9, the plots of $\ln[\beta \cdot g(\alpha)/(T-T_o)]$ versus $1/T$ at different heating rates (β_s) can be obtained by linear regression. The most probable mechanism function $g(\alpha)$ is the function that affords the most linear plot with a linear regression coefficient R^2 closest to 1.000.

The compensation effect [19] was used for accurate determination of the reaction model and pre-exponential factor, and the calculated E_i and A_i values from each of the models at different heating rates were substituted into Eq. 10 to determine the compensation effect parameters a and b.

$$\ln A_i = aE_i + b \tag{10}$$

The pre-exponential factor A_o was calculated by substitution of the calculated E_o from the model free method and the a and b parameters in Eq. 11:

$$\ln A_o = aE_o + b \tag{11}$$

The calculated results are presented in Table 3. The E_o and A_o values were substituted into Eq. 12:

$$f(\alpha) = \beta(\frac{d\alpha}{dT})_\alpha \, [A_o e^{\left(\frac{-E_o}{RT_\alpha}\right)}]^{-1} \tag{12}$$

Table 3. The kinetic triplet of AN/TU reaction in the presence and absence of nano metal oxide obtained by using model-fitting and compensation methods

Ignition reaction	β [K·min^{-1}]	Mechanism function, $g(\alpha)$	E_i [kJ·mol^{-1}]	ln A_i [min^{-1}]	R^2	E_o [kJ·mol^{-1}]	ln A_o [min^{-1}]	RSS
AN/TU/Mn_2O_3 mixture	5	$g(\alpha)=[-\ln(1-\alpha)]^{1/4}$	171.1	40.9	0.991	101.8	24.1	4.1
	10		127.4	30.2	0.982			3.0
	15		121.3	28.6	0.990			2.4
	20		85.7	20.3	0.991			1.4
AN/TU mixture	5	$g(\alpha)=[-\ln(1-\alpha)]^{1/3}$	110.5	25.9	0.998	110.1	26.0	0.72
	10		116.0	27.2	0.998			1.2
	15		147.1	34.3	0.999			1.1
	20		134.6	31.4	0.999			1.6

The calculated numerical values of $f(\alpha)$ were compared against the theoretical dependencies obtained from the $f(\alpha)$ equations (*e.g.* Table 3) to identify the best matching model. By applying this method to all of the reaction models, the mechanism function of Avrami-Erofeev A_4 ($g(\alpha) = [-\ln(1-\alpha)]^{1/4}$ and $f(\alpha) = 4(1-\alpha)[-\ln(1-\alpha)]^{3/4}$) and Avrami-Erofeev A_3 ($g(\alpha) = [-\ln(1-\alpha)]^{1/3}$ and $f(\alpha) = 3(1-\alpha)[-\ln(1-\alpha)]^{2/3}$) were found to be the best fits for the ignition reaction of AN/TU/Mn_2O_3 and AN/TU mixtures, respectively. Plots of the theoretical and experimental $f(\alpha)$ versus α at different heating rates for each of the reactions are presented in Figures 8 and 9.

The RSS (residual sum of squares) values that the show minimum difference between the experimental and theoretical values of $f(\alpha)$, presented in Table 3, verify the chosen reaction model. Based on these results, it can be concluded that the mechanism function with the integral forms $g(\alpha) = [-\ln(1-\alpha)]^{1/4}$ and

$g(\alpha) = [-\ln(1-\alpha)]^{1/3}$ are related to the reactions of AN/TU in the presence and absence of Mn_2O_3 nanoparticles, respectively. The difference between the reaction mechanisms proves that the presence of Mn_2O_3 nanoparticles changes the reaction route of AN/TU mixtures.

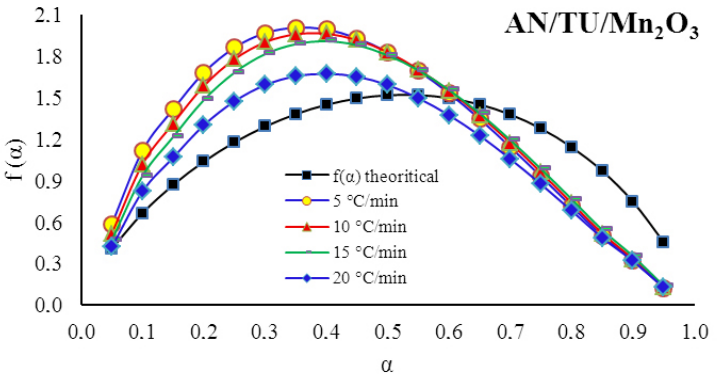

Figure 8. Plots of theoretical and experimental values of f(α) against various conversions (α = 0.05-0.95, with 0.05 increment) for reaction of AN/TU mixture in the presence of nano sized Mn_2O_3 at different heating rates

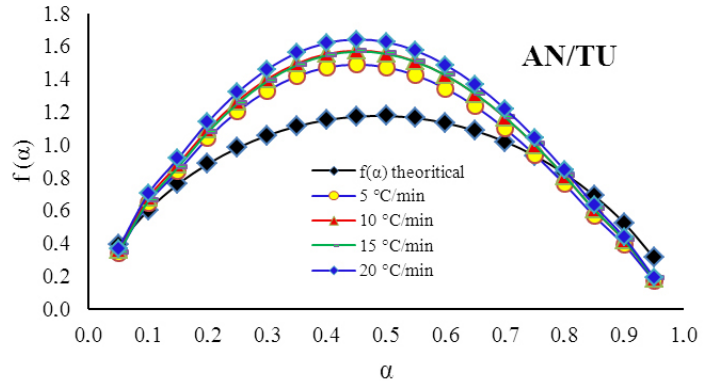

Figure 9. Plots of theoretical and experimental values of f(α) against various conversions (α = 0.05-0.95, with 0.05 increment) for reaction of AN/TU (50/50) mixture at different heating rates

4 Conclusions

In this study, we synthesized nano-sized Mn_2O_3 powder by a co-precipitation method. The metal oxide nanoparticles were characterized by XRD, SEM, and BET techniques and their effect on the ignition reaction of AN/TU mixture was investigated by the TG/DSC technique at different heating rates. The enthalpy studies indicated that the heat evolved from the ignition reaction in the presence of Mn_2O_3 nanoparticles was about 4 times that in the absence of the metal oxide. According to the results obtained, the ignition reaction equations of AN/TU in the presence and absence of Mn_2O_3 were suggested and verified by theoretical calculation of the reaction heat.

In order to reliably estimate the activation energy of ignition reactions, the KAS and Friedman methods were used. The mean values of the activation energies for α in the range 0.1-0.9 were 86.5 kJ·mol^{-1} to 101.8 kJ·mol^{-1} and 110.1 kJ·mol^{-1} to 117.3 kJ·mol^{-1} for the ignition reactions of AN/TU in the presence and absence of Mn_2O_3 nanoparticles, respectively. The results revealed that Mn_2O_3 nano oxide has catalytic activity on the ignition reaction of AN/TU mixtures. The catalytic activity of the Mn_2O_3 was described based on the electronic configuration of the metal cation.

The pre-exponential factor (A) and kinetic model function were determined by the compensation effect that associates model free and model fitting data to select the best model. By this method the Avrami-Erofeev mechanism functions A_4 and A_3 were assigned to describe the most probable mechanism for the AN/TU ignition reaction in the presence and absence of the studied nano-metal oxide, respectively.

Acknowledgement
We would like to thank the research committee of Malek-ashtar University of Technology (MUT) for supporting this work.

References

[1] Pouretedal, H. R.; Ravanbod, M. Kinetic Study of Ignition of Mg/$NaNO_3$ Pyrotechnic Using Non-isothermal TG/DSC Technique. *J. Therm. Anal. Calorim.* **2015**, *119*: 2281-2288.
[2] Conkling, J. A. *Chemistry of Pyrotechnics: Basic Principles and Theory*. 1st ed., Marcel Dekker Inc., New York **1985**, p. 51; ISBN 9781574447408.
[3] Izato, Y.; Miyake, A.; Date, S. Combustion Characteristics of Ammonium Nitrate

and Carbon Mixtures Based on a Thermal Decomposition Mechanism. *Propellants Explos. Pyrotech.* **2013**, *38*: 129-135.

[4] Zygmunt, B. Detonation Parameters of Mixtures Containing Ammonium Nitrate and Aluminium, *Cent. Eur. J. Energ. Mater.* **2009**, *6*: 57-66.

[5] Kajiyama, K.; Izato, Y.; Miyake, A. Thermal Characteristics of Ammonium Nitrate, Carbon, and Copper(II) Oxide Mixtures. *J. Therm. Anal. Calorim.* **2013**, *113*: 1475-1480.

[6] Oommen, C.; Jain, S. R. Ammonium Nitrate: A Promising Rocket Propellant Oxidizer. *J. Hazard. Mater.* **1999**, *67*: 253-281.

[7] Chaturvedi, S.; Dave, P. N. Review on Thermal Decomposition of Ammonium Nitrate. *J. Energ. Mater.* **2013**, *31*: 1-26.

[8] Wharton, R. K.; Barratt, A. J. Observations on the Reactivity of Pyrotechnic Compositions Containing Potassium Chlorate and Thiourea. *Propellants Explos. Pyrotech.* **1993**, *18*: 77-80.

[9] Czajka, B.; Foltynowicz, Z.; Wachowski, L. A Study of the Influence of Selected Transition Metals on the Solid State Reactivity in a Fe-$KClO_4$ Mixture. *Cent. Eur. J. Energ. Mater.* **2014**, *11*: 271-283.

[10] Babar, Z.; Malik, A. Q. Thermal Decomposition and Kinetic Evaluation of Composite Propellant Material Catalyzed with Nano Magnesium Oxide. *NUST Journal of Engineering Sciences* **2014**, *7*: 5-14.

[11] Ba, S.; Zhang, Z.; Yan, M.; Sun, Z.; Teng, X. Effect of Nano-CuO on Luminous Intensity of Pyrotechnics Composite Containing $KClO_4$ and Al. *Appl. Mech. Mater.* **2012**, *217-219*: 669-672.

[12] Martins, S.; Fernandes, J. B.; Mojumdar, S. C. Catalysed Thermal Decomposition of $KClO_3$ and Carbon Gasification. *J. Therm. Anal. Calorim.* **2015**, *119*: 831- 835.

[13] Kapoor, I. P. S.; Srivastava, P.; Singh, G. Nanocrystalline Transition Metal Oxides as Catalysts in the Thermal Decomposition of Ammonium Perchlorate. *Propellants Explos. Pyrotech.* **2009**, *34*: 351-356.

[14] Mahinroosta, M. Catalytic Effect of Commercial Nano-CuO and Nano-Fe_2O_3 on Thermal Decomposition of Ammonium Perchlorate. *J. Nanostruct. Chem.* **2013**, *3*: 1-6.

[15] Vyazovkin, S.; Burnham, A. K.; Criado, J. M.; Pérez-Maqueda, L. A.; Popescu, C.; Sbirrazzuoli, N. ICTAC Kinetics Committee Recommendations for Performing Kinetic Computations on Thermal Analysis Data. *Thermochim. Acta* **2011**, *520*: 1-19.

[16] Kissinger, H. E. Reaction Kinetics in Differential Thermal Analysis. *Anal. Chem.* **1957**, *29*: 1702-1706.

[17] Akahira, T.; Sunose, T. *Method of Determining Activation Deterioration Constant of Electrical Insulating Materials*. Research Report of Chiba Institute of Technology **1971**, *16*: 22-31.

[18] Friedman, H. L. Kinetics of Thermal Degradation of Char-forming Plastics from Thermogravimetry, Application to a Phenolic Plastic. *J. Polym. Sci., Part C: Polym. Symp.* **1964**, *6*: 183-195.

[19] ASTM E537-07, Standard Test Method for the Thermal Stability of Chemicals by Differential Scanning Calorimetry. *Annual Book of ASTM Standards*. Vol. 14.02, ASTM International, West Conshohocken, PA **2007**.
[20] Ravanbod, M.; Pouretedal, H. R. Catalytic Effect of Fe_2O_3, Mn_2O_3, and TiO_2 Nanoparticles on Thermal Decomposition of Potassium Nitrate. *J. Therm. Anal. Calorim.* **2016**, *124*: 1091-1098.
[21] Wang, Z. H.; Geng, D. Y.; Hu, W. J.; Ren, W.J.; Zhang, Z.D. Magnetic Properties and Exchange Bias in Mn_2O_3/Mn_3O_4 Nanoclusters. *J. Appl. Phys.* **2009**, *105*: 07A315/1-3.
[22] Scherrer, P. Bestimmung der Grosse und der Inneren Struktur von Kolloidteilchen Mittel Rontgenstrahlen, Nachrichten von der Gesellschaft der Wissenschaften. *Gottingen. Mathematisch Physikalische Klasse* **1918**, *2*: 98-100.
[23] SimoÄes, P. N.; Pedroso, L. M.; Portugala, A. A.; Campos, J. L. Study of the Decomposition of Phase Stabilized Ammonium Nitrate (PSAN) by Simultaneous Thermal Analysis: Determination of Kinetic Parameters. *Thermochim. Acta* **1998**, *319*: 55-65.
[24] Wang, S.; Gao, Q.; Wang, J. Thermodynamic Analysis of Decomposition of Thiourea and Thiourea Oxides. *J. Phys. Chem. B* **2005**, *109*: 17281-17289.
[25] Wang, Z. D.; Yoshida, M.; George, B. Theoretical Study on the Thermal Decomposition of Thiourea. *Comput. Theor. Chem.* **2013**, *1017*: 91-98.
[26] Luo, Y. R. *Comprehensive Handbook of Chemical Bond Energies*. CRC Press, Boca Raton, FL **2007**; ISBN 9780849373664.
[27] Pouretedal, H. R.; Damiri, S.; Ghaemi, E. F. Non-isothermal Studies on the Thermal Decomposition of C4 Explosive Using the TG/DTA Technique. *Cent. Eur. J. Energ. Mater.* **2014**, *11*: 405-416.
[28] Ren, Y. H.; Zhao, F. Q.; Yi, J. H.; Xu, K. Z.; Ma, H. X.; Hu, R. Z.; Song, J. R. Studies on an Ionic Compound $(3\text{-ATz})^+$ $(NTO)^-$: Crystal Structure, Specific Heat Capacity, Thermal Behaviors and Thermal Safety. *J. Iran. Chem. Soc.* **2012**, *9*: 407-414.
[29] Ravanbod, M.; Pouretedal, H. R.; Amini, M. K.; Ebadpour, R. Kinetic Study of the Thermal Decomposition of Potassium Chlorate Using the Non-isothermal TG/DSC Technique. *Cent. Eur. J. Energ. Mater.* **2016**, *13*: 505-525.
[30] Chaturvedi, S.; Dave, P. N. A Review on the Use of Nanometals as Catalysts for the Thermal Decomposition of Ammonium Perchlorate. *J. Saudi Chem. Soc.* **2013**, *17*: 135-149.
[31] Zhang, Y.; Kshirsagar, G.; Ellison, J. E. Catalytic Effects of Metal Oxides on the Thermal Decomposition of Sodium Chlorate. *Thermochim. Acta* **1993**, *228*: 147-154.
[32] Vargeese, A. A.; Muralidharan, K.; Krishnamurthy, V. N. Kinetics of Nano Titanium Dioxide Catalyzed Thermal Decomposition of Ammonium Nitrate and Ammonium Nitrate-based Composite Solid Propellant. *Propellants Explos. Pyrotech.* **2015**, *40*: 260-266.
[33] Kennedy, J. A.; Clark, S. M. A New Method for the Analysis of Non-isothermal DSC and Diffraction Data. *Thermochim. Acta* **1997**, *307*: 27-35.